Monte Carlo study of Ising model with non-integer effective dimensions

Synge TODO
Department of Physics, University of Tokyo, Tokyo, 113-0033
Institute for Solid State Physics, University of Tokyo, Kashiwa, 277-8581

Abstract

We review recent advances in the Markov-chain Monte Carlo method, especially the irreversible kernel and the $O(N)$ method based on the geometric allocation technique. After the review of the MCMC, we present the results of our recent Monte Carlo simulation of the Ising model with long-range interaction as well as the correlated random-field Ising model, both of which exhibits critical behavior with non-integer effective dimensions depending on the decay exponent of the long-range interaction or the spatial correlation of the random field.

1 Introduction

Critical phenomena are classified into "universality classes" according to their critical exponents. In general, the critical exponents depend on only a few basic properties of the system, such as the dimensionality, symmetry of the order parameter, etc. However, the existence of long-range interaction (LRI) and/or randomness may change the critical behavior [1]. Various materials exhibit nontrivial phenomena, in which the long-range nature of the interactions, such as the dipole-dipole interaction and the RKKY interaction, plays an essential role. The randomness also causes various nontrivial behavior such as the spin-glass transition, slow dynamics, etc [2]. As for the critical behavior, they also alter the universality class. Interestingly, this change of universality can be interpreted as a continuous change of the effective dimension of the system as seen below.

If a spin system has LRI, all possible pairs of spins interact with each other. The simplest and most fundamental LRI is the algebraically decaying Ising interaction, $\sim r^{-(d+\sigma)}$, where d is the dimension of the lattice and σ is the decay exponent. For σ smaller than the lower critical decay exponent, $\sigma_{\rm L}$, the phase transition is expected to belong to the mean-field universality class. Especially, in the limit of $d+\sigma \to 0$, the system becomes equivalent to the fully connected Ising model. On the other hand, when σ becomes larger than the upper critical decay exponent, $\sigma_{\rm U}$, the nearest-neighbor interaction dominates and the transition belongs to the short-range universality class. In the intermediate regime, $\sigma_{\rm L} < \sigma < \sigma_{\rm U}$, the critical exponents vary continuously as σ changes (Fig. 1). For the d-dimensional LRI system, this continuous change of the critical exponents can be interpreted as a continuous change of the effective dimension between d and the upper critical dimension [3].

Similarly, the presence of randomness often changes the effective dimension of the system as well. The random-field Ising model (RFIM) is one of the representative random systems, which has randomly distributed external field [4]. In contrast to the LRI, however, the random field generally decreases the effective dimension. Especially, near the upper critical dimension, it is predicted that the critical behavior of the d-dimensional RFIM is the same as the pure system in $(d-2)$ dimen-

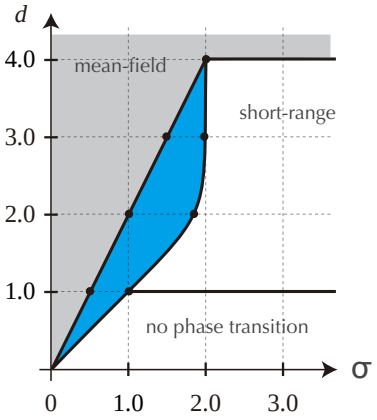

Figure 1: Schematic universality phase diagram of the Ising model with LRI. In the intermediate region, the effective dimension increases as σ decreases.

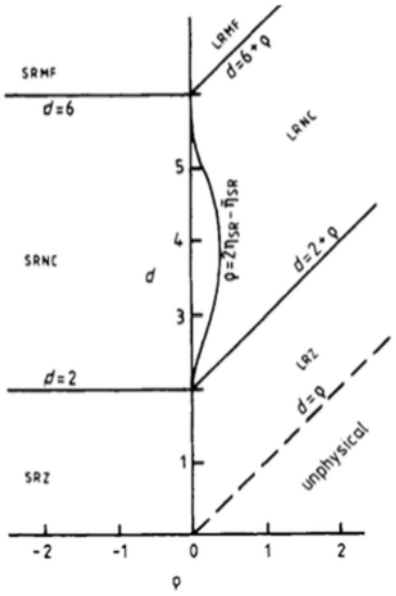

Figure 2: Schematic universality phase diagram of the $O(n)$ spin model with correlated random-field proposed (taken from Ref. [1]). For $\rho > 0$, the effective dimension decreases linearly as ρ increases.

sions. This phenomena is called "dimensional reduction" [5]. Moreover, it is expected that the spatial correlation between random fields can further decrease the effective dimension. For the spatial correlation that decreases algebraically with exponent $d - \rho$, the renormalization group study predicts that the upper critical dimension D_{U} and the lower critical dimension D_{L} become as $D_{\mathrm{U}} = d_{\mathrm{U}} + \rho$ and $D_{\mathrm{L}} = d_{\mathrm{L}} + \rho$, respectively, for $\rho \geq 0$, where $d_{\mathrm{U}} = 6$ and $d_{\mathrm{L}} = 2$ are those for uncorrelated random field [6]. This means that the effective dimension D of the d-dimensional RFIM with correlation exponent ρ is given by $d - \rho$, if we interpolate the effective dimension linearly between the lower and upper critical dimensions.

In this article, after a brief review of recent advances in the Markov-chain Monte Carlo method, we will present our results of extensive Monte Carlo simulation on the spin systems with LRI and the spatially correlated RFIM.

2 Advances in Markov-chain Monte Carlo method

The Markov-chain Monte Carlo (MCMC) method is one of the most powerful algorithms for numerical simulations in many research fields, such as the statistical physics, particle physics, chemistry, biology, informatics, finance, etc. In principle, the method can achieve statistically exact sampling asymptotically as long as the Markov chain satisfies the (total) balance and the ergodicity. Since the invention of the Metropolis algorithm in 1953, the detailed balance condition, a.k.a. reversibility, has been additionally imposed in most practical simulations as a sufficient condition for the total balance. Under the detailed balance condition, we enforce that every elementary transition should balance with its inverse process. Although a Markov chain satisfying the balance condition and ergodicity can generate random variables, or configurations, according to the target probability distribution, the MCMC method often suffers from strong correlation between successive samples in practice, which causes slow convergence and reduction in the effective number of samples. In other words, the strong autocorrelation may introduce systematic error as well as the increase of statistical error.

In generally, we should take the following five key points into account in order to achieve efficient MCMC sampling:

i) Representation (definition of "configurations").
ii) Choice of ensemble (weight of configurations).
iii) Generation of candidate configurations from the current configuration.
iv) Choice of transition kernel (probability), given a set of candidate configurations.
v) Algorithm for choosing a configuration according to transition probability.

From the viewpoint of the ergodicity, i), ii) and iii) are essential. In the quantum Monte Carlo method, for example, the non-local cluster update method [7], in which a world-line configuration is updated globally thorough a graph configuration, is often used. Another major technique is the worm algorithm [8, 9], where we introduce a pair of defects into the world-line configurations, to relax the strong restriction and recover the ergodicity. These techniques often reduce the correlation time drastically by orders of magnitude as well especially near the phase transition point.

More recently, from viewpoint iv), the importance of breaking the reversibility has been discussed intensively. In Ref. [9], we have shown that it is generally possible to construct an irreversible transition kernel by using the geometric allocation technique, and also that it can indeed reduce the auto-correlation drastically in many relevant cases by minimizing the rejection probability. The concept of breaking the reversibility can be applied not only to the elementary transition but also to the chain of events (or updates) [9, 10], where the global stochastic flow is introduced in the phase space and the Markov chain is further accelerated.

The technique of geometric allocation for the probability even improves the algorithm for choosing configuration [viewpoint v)]. Indeed, it is possible to draw a random number according to arbitrary probability distribution in a constant time by using Walker's method of aliases. This method, together with the space-time interchange technique, can reduce the computational time especially for the case where the number of candidates is large, such as models with LRI [11]. In the naive implementation of the Metropolis algorithm or the Swendsen-Wang algorithm, the total cost of one Monte Carlo step for N spins is proportional to N^2. However, since the interaction becomes weaker as the distance increases, one may reduce the computational cost from $O(N^2)$ to $O(N)$ without introducing any approximation [12]. The present $O(N)$ technique can be generalized to the quantum Monte Carlo method as well as the extended ensemble methods, such as the exchange Monte Carlo, multi-canonical method, and Wang-Landau sampling, etc.

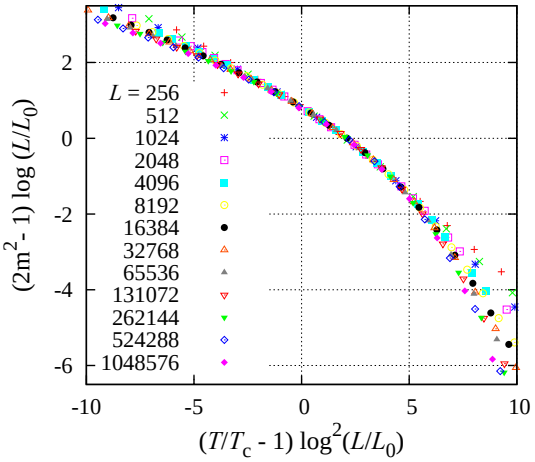

Figure 3: Scaling plot of the magnetization squared for the 1D transverse-field Ising model with $\sigma = 1$ and $\Gamma = 1$ (taken from Ref. [12]).

3 Ising model with long-range interaction

Transverse-field Ising model

In this section, we first consider the one-dimensional (1D) transverse-field Ising model,

whose Hamiltonian is defined as

$$\mathcal{H} = -\sum_{i<j} J_{ij}\sigma_i^z\sigma_j^z - \sum_i \Gamma\sigma_i^x \qquad (1)$$

with

$$J_{ij} = r_{ij}^{-(1+\sigma)}. \qquad (2)$$

In the absence of the transverse field, Γ, this model reduces to the classical Ising chain. In the classical case, the lower and upper critical decay exponents are known as $\sigma_{\rm L} = \frac{1}{2}$ and $\sigma_{\rm U} = 1$, respectively. When $\sigma > \sigma_{\rm U}$, there is no finite-temperature phase transition.

At $\sigma = \sigma_{\rm U}$, however, it is known that the system exhibits a Kosterlitz-Thouless (KT) phase transition at a finite temperature [13]. This KT transition is expected to persist, as long as Γ is sufficiently small. In Fig. 3, the system size and the temperature dependence of the magnetization squared, m^2, is shown for the quantum case, $\Gamma = 1$. Surprisingly, all the data with different system sizes (from $L = 2^8$ to 2^{20}) collapse on a single curve, by rescaling the temperature and the magnetization squared as $(T/T_{\rm c})\log^2(L/L_0)$ and $(2m^2 - 1)\log(L/L_0)$, where T is the temperature, and $T_{\rm c}$ and L_0 are determined as 1.38460(25) and 0.26(10), respectively, by using the least-squares fitting. This logarithmic scaling behavior strongly suggests that the KT transition in the classical case is robust against the quantum fluctuation, though the transition temperature becomes lower [$T_{\rm c} = 1.52780(9)$ for $\Gamma = 0$].

At critical transverse field $\Gamma_{\rm c}$, the finite-temperature KT transition vanishes, at which a quantum multicritical point emerges. By the finite-size scaling analysis, we evaluated as $\Gamma_{\rm c} \simeq 2.5236$, and found that the spin gap Δ and the susceptibility χ at $\Gamma_{\rm c}$ are scaled as $\Delta = L^{-z}f(L^zT)$ and $\chi = L^{\gamma}g(L^zT)$, respectively, with the dynamical exponent $z = 0.501$ and the exponent for the susceptibility $\gamma/\nu = 0.99$. These value are consistent with the predicted value $z = 0.5$ and $\gamma/\nu = 1$ by the renormalization group analysis [14].

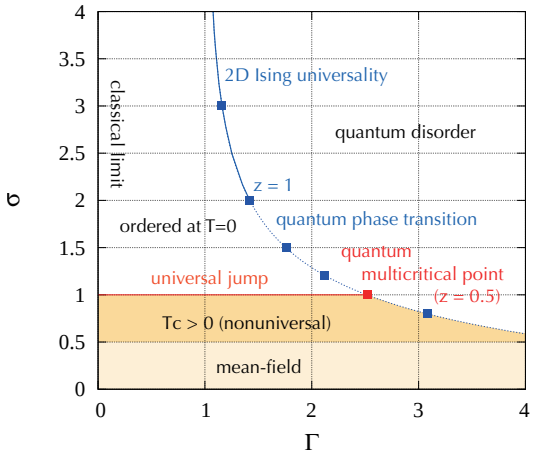

Figure 4: Ground-state phase diagram of the 1D transverse-field Ising model. In the shaded region, there occurs a finite-temperature transition.

In Fig. 4, we present the ground state phase diagram of the transverse field Ising model with LRI obtained by the quantum Monte Carlo simulation. In the limit of $\sigma = \infty$, the present model is reduced to the nearest neighbor Ising model, where the quantum phase transition of the classical two-dimensional (2D) Ising universality occurs at $\Gamma = 1$. As σ decreases, the critical transverse field increases. We found that, for $\sigma \geq 2$, the universality class of the quantum phase transition is the same as the 2D classical Ising universality, whereas the critical exponents, z and γ/ν, start to deviate continuously from the 2D classical Ising values for $\sigma < 2$.

Critical decay exponent in two dimensions

Nest, we discuss the classical 2D case ($d = 2$ and $\Gamma = 0$). While there is a consensus that $\sigma_{\rm L} = d/2 = 1$ in 2D, there still remain theoretical as well as numerical discussions about the upper critical decay exponent $\sigma_{\rm U}$ [15, 16, 17, 18, 19, 20, 21]. One of the largest difficulty in the numerical analysis of the present model is the large finite-size corrections to the scaling in the vicinity of the critical decay exponent. To overcome this problem,

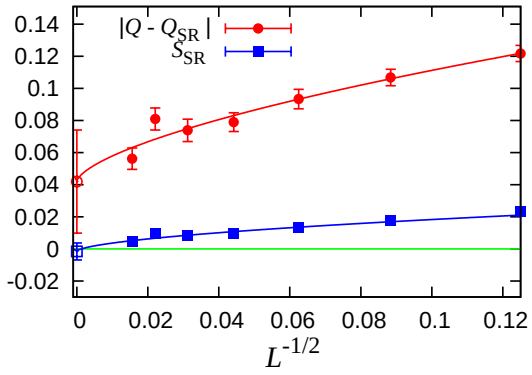

Figure 5: System-size dependence of the conventional Binder ratio Q and the self-combined Binder ratio $S_{\rm SR}$ at $\sigma = 7/4$. The solid lines denotes the result of least-squares fitting to $A + aL^{-b}$.

instead of the critical exponents, we use the value of the Binder ratio, $Q = \langle m^2\rangle^2/\langle m^4\rangle$. The Binder ratio at the critical point, which is also referred to as the universal ratio, does not depend on the system size and takes a universal value, since it is the ratio of two physical quantities that have the same anomalous dimension. It can be calculated more accurately than the critical exponents, which leads to more reliable identification of the universality class [22].

In order to further suppress the finite-size corrections, we introduce another quantity, named the "self-combined Binder ratio",

$$S(T,L) = \frac{1}{Q_\infty} Q(T,L) + Q_\infty \frac{1}{Q(T,L)} - 2, \tag{3}$$

where Q_∞ denotes the universal ratio. This quantity is a linear combination of Q and Q^{-1}. It is easily seen that regardless of the form of the correction term in Q at the critical point, the leading correction of the universal ratio is removed automatically if Q_∞ is chosen as the exact universal ratio [23]. Indeed, we already know the precise value of the universal ratio for the mean-field universality and the 2D short-range Ising universality as $Q_{\rm MF} = 0.456947$ and $Q_{\rm SR} = 0.856216$, respectively [24, 25].

By using the $O(N)$ Swendsen-Wang cluster algorithm [12], we simulate the 2D Ising model up to $L = 4096$ for $\sigma = 0.8, 0.9, \cdots, 1.9, 2.0$ and perform the finite-size scaling analysis. In Fig. 5, we show the system-size dependence of the (standard) Binder ratio Q and the self-combined Binder ratio $S_{\rm SR}$ at $\sigma = 7/4$. For the definition of $S_{\rm SR}$, we use the universal ratio for the short-range Ising universality, $Q_{\rm SR} = 0.856216$. We observe that the self-combined Binder ratio converges rapidly to zero. This strongly supports that the assumed value for Q_∞ is correct, that is, $\sigma = 7/4$ belongs to the short-range universality. We also confirmed that the extrapolated value of $S_{\rm SR}$ grows as $\sim (7/4 - \sigma)^2$ for $\sigma < 7/4$. Thus, we conclude that the upper critical decay exponent is $\sigma_{\rm U} = 7/4$ for $d = 2$ [23].

On the other hand, the conventional Binder ratio Q is extrapolated to some different value from $Q_{\rm SR}$. This is due to the existence of strong (likely logarithmic) corrections at the critical decay exponent. We also confirmed that at $\sigma = 1$, $S_{\rm MF}$ converges to zero, whereas Q shows slow convergence.

4 Random-field Ising model with spatial correlation

Correlated random field

In this section, we discuss the dimensional reduction in the random-field Ising model with spatial correlation. We consider the Gaussian random fields with algebraically long-range correlation,

$$P(h_i) = \frac{1}{\sqrt{2\pi} h_R} \exp[-h_i^2/2h_R^2] \tag{4}$$

$$C_{ij} = \langle\langle h_i h_j \rangle\rangle = \begin{cases} h_R^2 & \text{for } i = j \\ a h_R^2 / r_{ij}^{d-\rho} & \text{otherwise,} \end{cases} \tag{5}$$

where $\langle\langle \cdot \rangle\rangle$ denotes the average over the random field realizations. The random-field generation is accomplished by the decomposition of $(L^d \times L^d)$ correlation matrix C. Let us consider the factorization of the positive definite

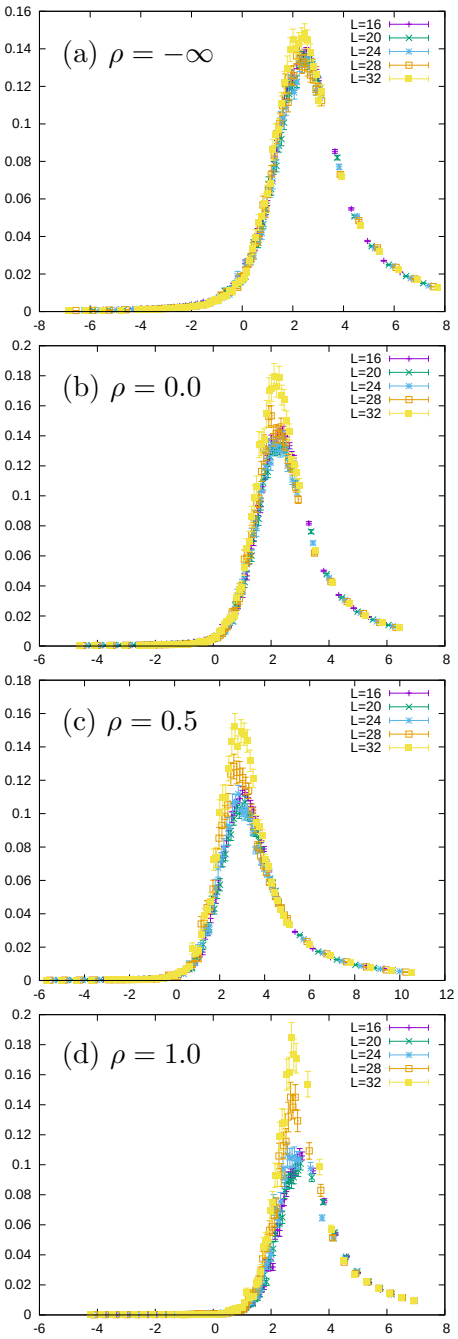

Figure 6: Scaling plot of the connected susceptibility of the 3D RFIM with (a) $\rho = -\infty$, (b) $\rho = 0.0$, (c) $\rho = 0.5$, and (d) $\rho = 1.0$.

symmetric matrix C into a matrix M and its transpose, $C = MM^T$. This factorization can be done by the Cholesky decomposition or the diagonalization. Once the matrix M is constructed, we can generate the correlated Gaussian random fields Y by multiplying the matrix M and a vector of independent standard Gaussian random numbers X as $Y = MX$. It is straightforward to confirm that the correlation between the components in Y is equal to C, i.e., $\langle\langle YY^T \rangle\rangle = C$. Note that the cost for the random field generation is proportional to L^{3d}. In this work, we use the parallel eigensolver via the Rokko Library [26] to generate 2^{20} samples of random field up to $L = 32$ and 14 for three-dimensional (3D) and four-dimensional (4D) cases, respectively.

Finite size scaling analysis

We calculated the specific heat, the connected and disconnected susceptibilities, the connected and disconnected Binder ratios, etc, by using the MCMC method. The connected and disconnected susceptibilities are defined by

$$\chi_{\rm con} = L^d \langle\langle \langle m^2 \rangle - \langle |m| \rangle^2 \rangle\rangle \qquad (6)$$

$$\chi_{\rm dis} = L^d [\langle\langle \langle |m| \rangle^2 \rangle\rangle - \langle\langle \langle |m| \rangle \rangle\rangle^2], \qquad (7)$$

respectively. The former represents the thermal fluctuations, whereas the latter does the random fluctuations. Accordingly, they are characterized by different critical exponents, γ and $\bar{\gamma}$, respectively.

In Fig. 6, we show the finite-size scaling plot of the connected susceptibility,

$$\chi_{\rm con} = L^{\gamma/\nu} \bar{\chi}_{\rm con}(L^{1/\nu}(T - T_{\rm c})) \qquad (8)$$

for the 3D RFIM with $\rho = -\infty$, 0.0, 0.5, and 1.0, from which the exponent γ and ν are estimated as listed in Table 1. We also performed similar analysis for the 4D RFIM with $\rho = -\infty$, 0.0, 0.5, 1.0, and 1.5. We found that the exponent γ increases gradually as ρ increases. This behavior is consistent with that the effective dimension decreases as ρ increases

Table 1: Critical exponents of the 3D and 4D RFIM obtained by the finite-size scaling analysis for the connected susceptibility.

d	ρ	T_c	ν	γ	D
3	$-\infty$	3.42(4)	1.4(2)	2.3(2)	1.3(1)
	0.0	3.55(6)	1.5(4)	2.5(7)	1.4(2)
	0.5	3.43(5)	1.5(3)	2.5(4)	0.8(3)
	1.0	3.17(9)	1.8(4)	3.0(2)	0.3(3)
4	$-\infty$	5.74(3)	0.8(1)	1.5(2)	2.0(2)
	0.0	5.82(6)	1.1(2)	2.1(3)	2.1(2)
	0.5	5.68(9)	1.3(3)	2.3(3)	1.7(2)
	1.0	5.5(2)	1.6(3)	2.6(4)	1.3(3)
	1.5	4.9(3)	2.3(6)	3.4(7)	1.0(1)

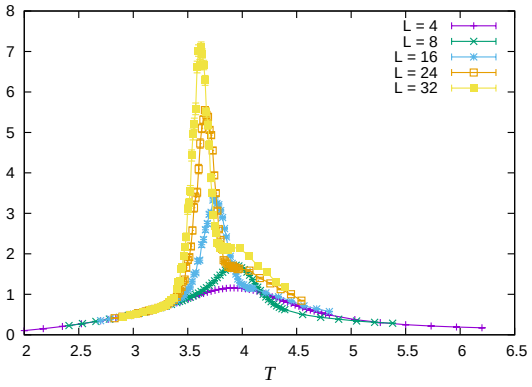

Figure 7: Temperature dependence of the specific heat of the 3D RFIM with $\rho = 0.5$. Growth of the second peak around $T \approx 4.0$ is clearly observed.

for $\rho \geq 0$ (cf. $\gamma = 1$, 1.2372, and 7/4 for the pure Ising model in four, three, and two dimensions, respectively). We observe the critical exponents for the 3D case with $\rho = 0.0$ agree with those for the 4D case with $\rho = 1.0$. This is again consistent with the previous theoretical prediction, $D = d - \rho$ at the upper and lower critical dimensions.

As seen clearly in Fig. 6, the finite-size scaling becomes worse as ρ increases. This might be due to the fact that the effective dimension approaches to the lower critical dimension, or becomes lower than that. Indeed, by using the scaling relation, $\eta = 2 - \gamma/\nu$ together with $D = d - \rho - 2 + \eta$, we can estimate the effective dimension of the criticality as presented in Table 1. The effective dimension is the same for $\rho = -\infty$ and 0.0, and starts to decrease both in the 3D and 4D cases as expected, and it becomes smaller than the lower critical dimension, $D = 1$, for 3D case with $\rho = 1.0$.

Finally, we mention the double peak structure of the specific heat. In Fig. 7, we show the temperature dependence of the specific heat of the 3D RFIM with $\rho = 0.5$. The sharper peak at lower temperature corresponds to the phase transition to the ordered phase. However, we observe that for sufficiently large ρ an extra peak appears at higher temperature. The weird double peak behavior may manifest another critical behavior at higher temperature [27], though we have no solid explanation for for the moment,

5 Summary

In this article, we have reviewed the recent advances in the Markov-chain Monte Carlo method, especially the irreversible kernel and the $O(N)$ method based on the geometric allocation technique. We present the results of our recent Monte Carlo study on the Ising model with long-range interaction as well as the correlated random-field Ising model, both of which exhibits critical behavior with non-integer effective dimensions depending on the decay exponent of the interaction or the spatial correlation of the random field. We established the upper and lower critical decay exponent for the 2D Ising model with LRI by using the $O(N)$ cluster Monte Carlo method together with the self-combined Binder ratio. For the correlated RFIM, we also observed that the effective dimension of the universality becomes small as the decay exponent increased. However, by the present accuracy of the MCMC simulation, we can not determine the critical decay exponent of the spatial correlation, at which the effective dimension becomes unity and thus the finite-temperature phase transition vanishes. This

is due to the lack of efficient MCMC method for the system with random field. A further development of the MCMC technique for such systems with lower symmetry is strongly demanded.

Acknowledgment

The author acknowledge the collaboration with T. Horita and H. Suwa. The simulation code used in the present study has been developed on the ALPS Library [28, 29] and the Rokko Library [26].

References

[1] A. J. Bray: J. Phys. C **19** (1986) 6225.

[2] D. S. Fisher: Phys. Rev. Lett. **56** (1986) 416.

[3] M. E. Fisher, S.-K. Ma, and B. G. Nickel: Phys. Rev. Lett. **29** (1972) 917.

[4] Y. Imry and S. K. Ma: Phys. Rev. Lett. **35** (1975) 1399.

[5] A. Aharony, Y. Imry, and S. K. Ma: Phys. Rev. Lett. **37** (1976) 1364.

[6] M. Kardar, B. McClain, and C. Taylor: Phys. Rev. B **27** (1983) 5875.

[7] S. Todo: *Strongly Correlated Systems: Numerical Methods (Springer Series in Solid-State Sciences)*, ed. A. Avella and F. Mancini (Springer-Verlag, Berlin, 2013) pp. 153–184.

[8] O. F. Syljuasen and A. W. Sandvik: Phys. Rev. E **66** (2002) 046701.

[9] H. Suwa and S. Todo: Phys. Rev. Lett. **105** (2010) 120603.

[10] M. Michel, S. C. Kapfer, and W. Krauth: J. Chem. Phys. **140** (2014) 054116.

[11] S. Todo and H. Suwa: J. Phys.: Conf. Ser. **473** (2013) 012013.

[12] K. Fukui and S. Todo: J. Comp. Phys. **228** (2009) 2629.

[13] P. W. Anderson and G. Yuval: J. Phys. C **4** (1971) 607.

[14] A. Dutta and J. K. Bhattacharjee: Phys. Rev. B **64** (2001) 184106.

[15] J. Sak: Phys. Rev. B **8** (1973) 281.

[16] A. C. D. van Enter: Phys. Rev. B **26** (1982) 1336.

[17] E. Luijten and H. W. J. Blöte: Phys. Rev. Lett. **89** (2002) 025703.

[18] M. Picco: arXiv:1207.1018.

[19] T. Blanchard, M. Picco, and M. A. Rajabpour: Europhys. Lett. **101** (2013) 56003.

[20] M. C. Angelini, G. Parisi, and F. Ricci-Tersenghi: Phys. Rev. E **89** (2014) 062120.

[21] N. Defenu, A. Trombettoni, and A. Codello: Phys. Rev. E **92** (2015) 052113.

[22] S. Yasuda and S. Todo: Phys. Rev. E **88** (2013) 061301(R).

[23] T. Horita, H. Suwa, and S. Todo: Phys. Rev. E **95** (2017) 012143.

[24] E. Luijten and H. W. J. Blöte: Int. J. Mod. Phys. C **6** (1995) 359.

[25] G. Kamieniarz and H. W. J. Blöte: J. Phys. A: Math. Gen. **26** (1993) 201.

[26] https://github.com/t-sakashita/rokko/.

[27] R. Sacconi: J. Phys. A: Math. Gen. **31** (1997) 3751.

[28] B. Bauer, L. D. Carr, H. G. Evertz, A. Feiguin, J. Freire, S. Fuchs, L. Gamper, J. Gukelberger, E. Gull, S. Guertler, A. Hehn, R. Igarashi, S. V. Isakov, D. Koop, P. N. Ma, P. Mates, H. Matsuo, O. Parcollet, G. Pawlowski, J. D. Picon, L. Pollet, E. Santos, V. W. Scarola, U. Schollwöck, C. Silva, B. Surer, S. Todo, S. Trebst, M. Troyer, M. L. Wall, P. Werner, and S. Wessel: J. Stat. Mech.: Theo. Exp. (2011) P05001.

[29] http://alps.comp-phys.org/.